

Published in final edited form as:

*Acad Radiol.* 2008 June ; 15(6): 753–762. doi:10.1016/j.acra.2007.10.019.

## Evaluation of structure-function relationships in asthma using multi-detector CT (MDCT) and hyperpolarized (HP) He-3 MRI

Sean B. Fain<sup>1,2,3</sup>, Guillermo Gonzalez-Fernandez<sup>4</sup>, Eric T Peterson<sup>3</sup>, Michael D. Evans<sup>5</sup>, Ronald L. Sorkness<sup>6</sup>, Nizar N. Jarjour<sup>6,7</sup>, William W. Busse<sup>6,7</sup>, and Janet E. Kuhlman<sup>2</sup>

<sup>1</sup> Medical Physics, University of Wisconsin – Madison, USA

<sup>2</sup> Radiology, UW Hospital, University of Wisconsin – Madison, USA

<sup>3</sup> Biomedical Engineering, University of Wisconsin – Madison, USA

<sup>4</sup> Electrical and Computer Engineering, University of Wisconsin – Madison, USA

<sup>5</sup> Biostatistics and Medical Informatics, University of Wisconsin – Madison, USA

<sup>6</sup> Morris Institute for Respiratory Research, University of Wisconsin – Madison, USA

<sup>7</sup> Department of Medicine, University of Wisconsin – Madison, USA

### Abstract

**Rationale and Objectives**—While multiple detector CT (MDCT) and hyperpolarized gas MRI (HP MRI) have demonstrated ability to detect structural and ventilation abnormalities in asthma, few studies have sought to exploit or cross-validate the regional information provided by these techniques. The purpose of this work is to assess regional disease in asthma by evaluating the association of sites of ventilation defect on HP MRI with other regional markers of airway disease, including air trapping on MDCT and inflammatory markers on bronchoscopy.

**Materials and Methods**—Both HP MRI using helium-3 and MDCT were acquired in the same patients. Supervised segmentation of the lung lobes on MRI and MDCT facilitated regional comparisons of ventilation abnormalities in the lung parenchyma. The percentage of spatial overlap was evaluated between regions of ventilation defect on HP MRI and hyperlucency on MDCT to determine associations between obstruction and likely regions of gas trapping. Similarly, lung lobes with high defect volume were compared to lobes with low defect volume for differences in inflammatory cell number and percentage using bronchoscopic assessment.

**Results**—There was significant overlap between sites of ventilation defect on HP MRI and hyperlucency on MDCT suggesting that sites of airway obstruction and air trapping are associated in asthma. The percent ( $r = 0.68$ ;  $p = 0.0039$ ) and absolute ( $r = 0.61$ ;  $p = 0.0125$ ) number of neutrophils on bronchoalveolar lavage (BAL) for the sampled lung lobe also directly correlated with increased defect volume.

**Conclusion**—These results show promise for using image guidance to assess specific regions of ventilation defect or air trapping in heterogeneous obstructive lung diseases such as asthma.

---

Corresponding Author: Sean B. Fain, PhD, J5/M158 CSC, Department of Radiology, University of Wisconsin Hospital, Madison, WI 53792.

**Publisher's Disclaimer:** This is a PDF file of an unedited manuscript that has been accepted for publication. As a service to our customers we are providing this early version of the manuscript. The manuscript will undergo copyediting, typesetting, and review of the resulting proof before it is published in its final citable form. Please note that during the production process errors may be discovered which could affect the content, and all legal disclaimers that apply to the journal pertain.

## Keywords

asthma; functional imaging; lungs; hyperpolarized gas; MRI; MDCT

---

## Introduction

Asthma affects millions of people world-wide and trends indicate increasing incidence, especially in children (1,2). Subjects with asthma experience periodic wheezing and shortness of breath that manifests on pulmonary function tests as reduced forced expiratory lung volume in 1 second (FEV1) and increased lung residual volume normalized to the total lung capacity (RV/TLC) compared to normal subjects. Bronchodilation with beta agonists such as albuterol can partially reverse this obstructive physiology by relaxing airway smooth muscle, but evidence from airway biopsies suggests that obstruction is also accompanied by chronic inflammation and airway remodeling (3).

Functional imaging in the lungs has great potential for mechanistic studies of lung disease, particularly for identifying regional patterns of obstruction that test physiologic hypotheses (4–7). Regional mosaics of reduced parenchymal density, apparently due to air trapping, are associated with asthma on computed tomography (CT) (8). More recently CT, and especially multi-detector CT (MDCT), have been used to quantitatively measure lung parenchymal density and correlate these measures to obstructive physiology (9,10).

Regional patterns of ventilation in asthma have also been explored using inhaled gas contrast agents in conjunction with imaging (11–14), including hyperpolarized helium-3 magnetic resonance imaging (HP MRI) (15). Like MDCT measures of parenchymal density, whole lung measures of ventilatory defect number on HP MRI correlate with obstructive physiology (7, 14,16). Recently, a substantial fraction of the regions of ventilation defect were shown to persist on repeated HP MRI studies of asthma patients separated in time by 1 week to more than one year (16). Similarly, whole lung images of ventilation acquired with HP MRI can be used to localize and quantify the percentage of ventilation defect over the whole lung (17) and potentially by lung lobe. Structure and function assessment of parenchymal density near regions of ventilation defect is therefore possible by combining the MDCT and HP MR imaging techniques.

The pathogenesis of airway obstruction in asthma involves smooth muscle hyperreactivity, inflammation and airway remodeling. Several studies suggest spatially heterogeneous patterns of ventilation that may be driven by local differences in structure and function. The hypothesis of this work is that imaging can provide a means to guide regional assessment of airway abnormalities to better identify regions of more intense disease in the lungs. Imaging can therefore provide a valuable tool to better assess mechanisms and distinguish different phenotypes of obstructive lung disease. Data from HP MRI and MDCT of the lungs in the same subjects with mild to moderate and severe asthma are compared with whole lung measures of physiology and with each other to explore the spatial correspondence of features of air trapping, ventilation defect, and inflammation.

## Materials and Methods

Our study was approved by our Institutional Review Board and was compliant with the Health Insurance Portability and Accountability Act (HIPAA). The inhalation of hyperpolarized <sup>3</sup>He gas for MRI is regulated as NC100182. Our studies were conducted under an investigational new drug (IND #64,687) protocol approved by the FDA. A total of 45 subjects with asthma (29 ± 10 years; 19 males and 26 females) underwent MDCT of the lungs at two different lung

volumes: full inspiration and at end-expiration, corresponding to total lung capacity (TLC), and functional residual capacity (FRC) respectively. These subjects were included in the study based on prior history of asthma using the criteria set forth by the expert panel of the National Institutes of Health (18), including reversibility of 12% or greater (at least 200 ml) after bronchodilation or methacholine reactivity with a provocative concentration causing a 20% decrease in FEV<sub>1</sub>(PC20) of <8 mg/ml. Exclusion criteria included upper respiratory infection within 2 weeks, > 5 pack years of smoking history, or a smoker in the past year. If a subject had previously smoked, a diffusion capacity was measured to ensure that it was >70% predicted. For added safety due to concerns about inhalation of the anoxic <sup>3</sup>He/N<sub>2</sub> gas mixture, subjects were excluded from HP MRI if their percentage of predicted forced expiratory volume at 1 second (FEV<sub>1</sub>% predicted) was less than 60%.

A subset of 21 of 45 (47%) subjects (30 ± 11 years; 9 males and 12 females) who underwent MDCT were also imaged with HP MRI and were analyzed for severity of *regional* ventilation defects and their correspondence to regions of focal air trapping on MDCT. A total of 6 of these 21 (29 %) subjects were further characterized as severe asthmatics based on the criteria set forth in the Severe Asthma Research Program (SARP) (19) - these include as a chief criterion the prolonged use of high dose corticosteroids to control symptoms (>880 mc).

### Pulmonary Function and Bronchoscopy

Spirometry and plethysmographic lung volume measurements were performed in all subjects according to ATS/ERS guidelines (20,21). Subjects withheld short-acting beta agonist treatments for 4 hours, long-acting beta agonist treatments for 12 hours, and other bronchodilator medications for an appropriate length of time to avoid interference with the measurements. The FEV<sub>1</sub> acquired immediately before MRI was used as the subject's baseline FEV<sub>1</sub> for analysis in all cases. Predicted values for FEV<sub>1</sub>, forced vital capacity (FVC), FEV<sub>1</sub>/FVC ratio, and forced expiratory flow rate at 25–75% FVC (FEF<sub>25–75</sub>) were computed using the equations of Hankinson, et al (22). Predicted values for total lung capacity (TLC), functional residual capacity (FRC), FRC/TLC ratio, residual volume (RV) and RV/TLC ratio were computed using the equations of Stocks and Quanjer (23), with adjustments for African Americans per ATS recommendations (24). Plethysmography measures were acquired 1–4 weeks prior to HP MRI.

Bronchoscopic assessment was performed in 16 of 21 (76 %) subjects within 1 week of imaging. Bronchoalveolar lavage (BAL) was acquired in a specific lobe, usually the right middle or right upper lobe, and inflammatory cell markers; including absolute and percent neutrophils, eosinophils, and macrophages; were retrospectively compared to the percentage of defect volume for the sampled lobe.

### Image Acquisition

MRI and MDCT acquisitions were performed within 48–72 hours of each other. Bronchoscopy was performed within 1 week of the last imaging study, usually CT. The time varied due to the logistical challenges of reconciling subjects' schedules with clinical openings and scanner availability.

In all subjects multi-detector (MDCT) imaging was performed using a GE Light Speed CT scanner with 16 or 64 detectors (GE Medical systems, Milwaukee, WI). For MDCT imaging three scans were acquired, each in a breath-hold of ~4 s: a low resolution scout scan followed by two high resolution scans, one at TLC followed by one at FRC. Two 3D lung volumes were then reconstructed, one at 0.625 mm slice thickness for quantitative measurement at nearly isotropic voxel size, and one at 5 mm slice thickness for qualitative evaluation and registration

to MRI. Other specific acquisition and reconstruction parameters used for MDCT data were as summarized in Table 1.

MR imaging was performed using a 1.5 T MR scanner with broadband capabilities (Signa LX, GE Medical systems, Milwaukee, WI). MR imaging for each subject included two conventional proton scans using the system's Body RF-coil: a T1-weighted scout localizer followed by a single shot 2D multi-slice fast spin echo (FSE) breath-held acquisition in the axial plane with field of view (FOV), slice thickness, and position matching the subsequent HP MRI scan. Prior to the FSE acquisition, the subject inhaled a volume of air equivalent to the volume of  $^3\text{He}/\text{N}_2$  mixture to be inhaled in order to match the position of the diaphragm for both scans.

For the  $^3\text{He}$  MRI scan a helium polarizer (IGI.9600, GE Healthcare) located adjacent to the MR scanner used the spin exchange optical pumping method to polarize  $^3\text{He}$  to 30–40%. The hyperpolarized gas contrast agent was a mixture of  $^3\text{He}$  and  $\text{N}_2$  with a net activity of polarized  $^3\text{He}$  of 4.5 mM. The  $^3\text{He}/\text{N}_2$  mixture was prepared by mixing 200–300 ml of 30–40% polarized  $^3\text{He}$  with nitrogen gas added to reach a total volume equivalent to 15% of the subject's TLC. This mixture was added to a tedlar bag (Jensen Inert Inc., Coral Springs, Florida, USA) that had been purged and rinsed with nitrogen to remove oxygen. The polarized gas was inhaled by the subject through an attached 1/8" Tygon tube (US Plastic Corp., Lima, Ohio, USA) starting with their lung volume at FRC.

A vest RF coil (IGC-Medical Advances, Milwaukee, WI) tuned to operate at the resonant frequency of  $^3\text{He}$  and decoupled from the Body RF-coil was used so that HP MRI and proton MRI could be acquired without moving the subject. A short 1–2 s scan was used in conjunction with a ~100 ml sip of  $^3\text{He}$  to determine center frequency and flip angle using the method outlined in Ref (25). The HP MRI ventilation acquisition consisted of a fast 2D multi-slice gradient echo breath-held acquisition in the axial plane with  $128 \times 128$  acquired matrix. The slice number for both FSE and HP MRI ranged between 13–19 slices to achieve whole lung (superior to inferior) coverage. Other specific imaging parameters are as summarized in Table 2. Electrocardiogram (ECG) and oxygen saturation ( $\text{saO}_2$ ) signals were monitored throughout the imaging session.

### Image Measurement

Whole lung air trapping on MDCT was quantitatively evaluated by calculating the percent of the lung volume falling below the thresholds of -850, -910 and -950 Hounsfield Units (HU) on expiratory CT. Additionally, focal regions of hyperlucency on MDCT were scored according to size and percentage of spatial overlap with regional ventilation defects on HP MRI in order to test for similar regional patterns of air trapping and obstruction.. The MRI and CT data were evaluated separately for size and location of ventilation defects on HP MRI and regions of hyperlucency based on the expiratory CT images respectively. After identifying these regions, the radiologist then assessed their degree of overlap using a 4 point scale. The 4 point scale assigned a value of 0 for no overlap, 1 for 26–50% overlap, 2 for 51–75 %, and 3 if >75% overlap.

For whole lung comparisons to pulmonary function, a discrete score similar to that used in ref (14) was used to measure ventilation defect number on HP MRI. A radiologist (JEK) evaluated the extent and location of defects by slice. If a defect was identified in a given slice, it was assigned a score based on its extent within that slice: 1 if  $\leq 25\%$ , 2 if between 26–50%, 3 if between 51–75 %, and 4 if >75%. The total lung defect score was calculated by summing the score over each slice. The minimum defect score was therefore zero, but the maximum depended on the total number defects observed.

For regional comparisons, a quantitative and continuous measure of the percent defect volume (% Defect Volume) for each lung lobe was calculated in a manner similar to that described in Ref (17). In contrast to previous studies, the defect volume was assessed for each lung lobe by displaying both MRI and inspiratory MDCT images for each subject in spatial registration (Fig 1ab) in a graphic user interface (Fig. 1c) written in Matlab 7.0 (The Mathworks, Natick, MA). The lung lobes and defect regions were segmented manually from the proton MR and HP MR images respectively by combining thresholding along with display of the lobe boundaries on MDCT images. This analysis resulted in a defect mask and a lobe volume mask that exploited the inherent spatial registration of the helium and proton MR images to calculate the defect volume by simply multiplying the two masks and summing the result..

### Statistical Analyses

The study design compared whole lung measures of ventilation defects on HP MRI and sites of hyperlucency on MDCT with pulmonary function measures of obstructive physiology. The volume and regional association of ventilation defects on HP MRI and sites of hyperlucency on MDCT were also compared on a whole lung and regional basis. The Spearman rank correlation was used to test for associations between image measures and pulmonary function measures. The Wilcoxon rank sum test was used to measure differences between groups. McNemar's test was used to assess regional overlap of airway abnormalities on imaging.

### Results

No adverse events occurred during MRI studies. The  $saO_2$  for all subjects remained above 90% in all cases, recovering to pre- $^3He$  inhalation levels within 5–10 seconds after the end of the breath-hold. Pulmonary function measures using spirometry and plethysmography were not significantly different for severe vs. non-severe subjects included in this study. However, the  $FEV_1$  % predicted (%p) tended to be lower in severe versus non-severe subjects ( $p = 0.055$ ) (Table 3). Significant correlations between image metrics and whole lung measures of pulmonary function are summarized in Table 4.

### MDCT Measures

Densitometry for the  $-850$  HU threshold on expiratory CT correlated (Table 4) directly with  $RV/TLC\%p$  ( $r = 0.53$ ,  $p = 0.003$ ), but this relationship did not hold for thresholds at  $-910$  and  $-950$ . There was not significantly different densitometry for severe vs. non-severe subjects ( $p = 0.61$ ) on MDCT (Table 3), but nor was there significantly different  $RV/TLC\%p$  for these groups.

### MRI Measures

On HP MRI, the number of ventilation defects correlated inversely with  $FEV_1\%p$  ( $r = -0.76$ ,  $p = 0.0002$ ). There was no significant difference in ventilation defect score for severe vs. non-severe subjects ( $p = 0.54$ ).

Regionally, ventilation defect volume was larger in the right middle lobe compared to the right upper ( $p = 0.002$ ) and right lower lobes ( $p = 0.008$ ). Severe subjects showed a higher defect volume in the left lower lobe ( $p = 0.02$ ) compared to non-severe subjects. The % Defect Volume burden at the site of bronchoscopic assessment correlated directly with both absolute ( $r = 0.61$ ;  $p = 0.0125$ ) and percent neutrophil ( $r = 0.68$ ;  $p = 0.0039$ ) counts in the BAL, while whole lung measures of percent defect volume did not correlate significantly with BAL neutrophil number ( $r = 0.30$ ;  $p = 0.27$ ) or percentage ( $r = 0.41$   $p = 0.11$ ). In addition, highly defecting lobes ( $\geq 10\%$  Defect Volume) also showed greater absolute ( $p = 0.05$ ) and percentage ( $p = 0.03$ ) neutrophils (Fig. 2) compared to less defecting lobes ( $< 10\%$  Defect Volume). There was no relationship

between the total number or percentage of eosinophils or macrophages and the defect measures on MRI.

### MDCT and MR Comparison

HP MRI and MDCT defects were found to be related overall ( $p=0.04$ ) and specifically for the right upper lobe ( $p=0.003$ ), left upper lobe ( $p=0.03$ ), and right middle lobe ( $p=0.04$ ). A typical example in the left lower lobe is shown in Figure 3. Qualitatively, there was greater correspondence between HP MRI defects and MDCT defects in severe asthma subjects compared to non-severe subjects (Fig. 4).

### Discussion

This work evaluates the physiological significance of two image metrics of obstructive lung disease that have been established in previous studies (8,9,14) to correlated with whole lung measures of airway obstruction and air trapping. In the present study, ventilation defects on HP MRI and hyperlucency on MDCT were also shown to correlate with whole lung measures of obstruction and air trapping respectively. In addition both image measures were found to be regionally associated, suggesting a possible shared mechanism underlying airway obstruction and air trapping. Moreover, inflammatory cell markers from BAL were shown to be elevated in lobes with a large defect volume percentage compared to lobes with low defect volume percentage, consistent with elevated inflammatory processes near locations of airway obstruction.

These regional relationships suggest that locations of air trapping and obstruction might correlate to regions of structural anomaly that make airways prone to collapse at lower lung volumes. Specifically, focal regions of hyperlucency suggestive of air trapping on CT were found to spatially overlap with regions of ventilation defect on MRI, suggestive that similar mechanical features of the airways in these regions may drive both abnormalities. For example, the lung volumes at image acquisition differ by  $\sim 1L$ , ranging from FRC for the expiratory MDCT to  $\sim 1L$  above FRC for the HP MRI data. By definition, ventilation defect regions on HP MRI presented with diminished intensity with respect to surrounding lung parenchyma. These regions only rarely demonstrate a complete absence of signal. Therefore the data suggest that, on average, ventilation defect regions above FRC on HP MRI represent partially obstructed airways that fully collapse at FRC resulting in air trapping in this study population. Finally, the defect burden in lung lobes corresponding to the site of BAL had higher total and percent neutrophils compared to less defected lobes, suggestive of increased inflammation at sites of increased airway obstruction.

For the image markers used in this study, there were no clear differences between severe and non-severe asthmatics. This likely points to several limitations of the present study, including the small sample size and the exclusion criterion of  $FEV1 < 60\%$ , which may have selected for a severe asthma population with minimal or modest baseline obstruction that is not necessarily representative of the Severe Asthma group in the SARP database. Also, although the MR and CT images were read separately by the radiologist, they were read in succession, and thus the radiologist was not blinded to the previous analysis. A blinded, or preferably quantitative, analysis of spatial overlap would be more desirable. To address this limitation, a lobar segmentation of the expiratory MDCT data is being developed to more easily allow quantitative assessment of overlap between MR and MDCT. An additional limitation was that the bronchoscopic assessment of lobar defects was retrospective – lobes in *different* subjects were compared for differences in BAL inflammatory cell counts. Prospective studies using imaging to guide bronchoscopic assessment at both a defected lobe and non-defected lobe in the *same* subject are needed to verify the regional association of inflammation as compared to the possibility of diffuse inflammation throughout the lungs. However, the lack of a strong

correlation between whole lung defect volume and inflammatory cell markers argues in favor of a stronger regional effect. Neutrophils are the cellular infiltrate found in acute episodes of asthma and in subclasses of patients with severe asthma. Therefore, the presence of elevated neutrophil levels might be expected. However, it is somewhat surprising that in our analysis of the relationship between the structural changes and inflammatory pattern, eosinophils did not correlate with regions of defect or hyperlucency. It is unclear whether this is a result of the patient population or if ventilation defects on MRI manifest due to a more acute inflammatory process. In addition, it is also of interest to compare large airway morphology, such as airway wall thickness, and lumen area, as a function of defect burden. Although this is outside the scope of the present work, the tools to perform these measurements at specific airway bronchi are commercially available, and a careful analysis of these regional relationships is ongoing.

Non-invasive markers of obstructive lung disease are needed to characterize mechanisms and therapies in asthma and COPD. Because of the observed spatial correspondence of abnormalities on MDCT and HP MRI, this work is also suggestive that regional hyperlucency on MDCT is a promising regional marker of airway obstruction that could provide a useful means to guide bronchoscopic assessment of the airways in ongoing mechanistic studies of asthma. At present, the MDCT imaging modality has advantages over HP MRI for image guidance studies, principally in its ability to depict both airway structure and regions of air trapping at FRC in 3D with high, nearly isotropic, spatial resolution. However, the ability of HP MRI to depict dynamic processes (26,27) is a key strength and new methods for 3D dynamic hyperpolarized gas MRI are being introduced (7). These techniques provide spatial resolutions approaching that of CT in addition to information about respiratory dynamics at the level of the individual airways (28).

In conclusion, we have shown that established markers of obstructive lung disease correlate to obstructive physiology and that regional patterns of airway abnormality agree on MDCT and HP MRI. The increased neutrophils in BAL fluids sampled at locations of high ventilation defect suggest a regional association of inflammation and ventilation defects on MR imaging. However, prospective comparisons of image markers and cellular markers of inflammation using an image-guided bronchoscopic approach to sample multiple locations in the lungs of the same subject are necessary to confirm these results.

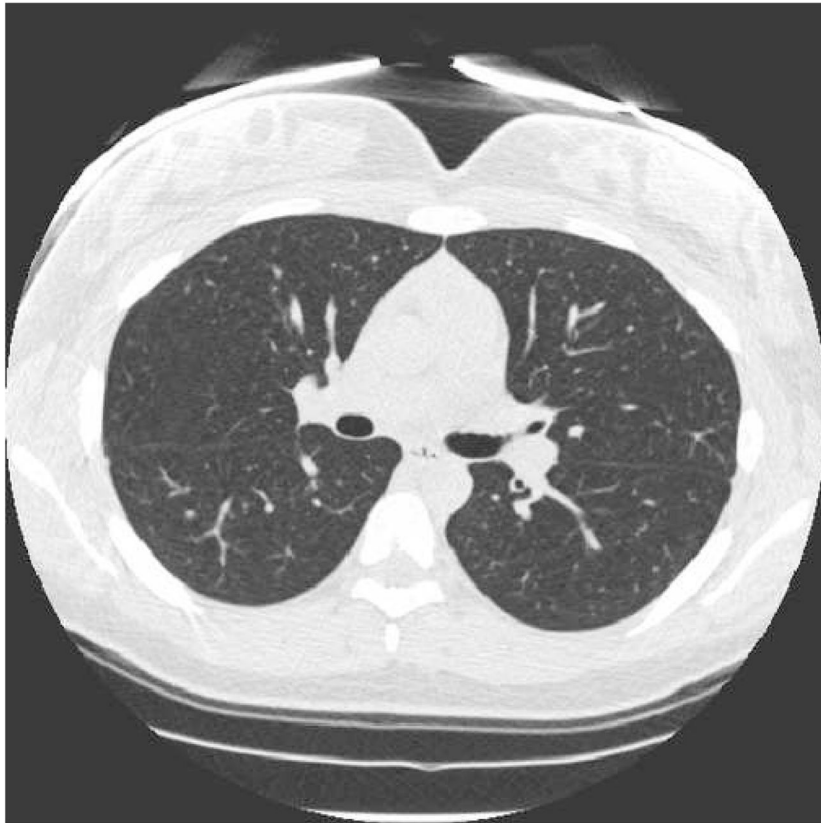
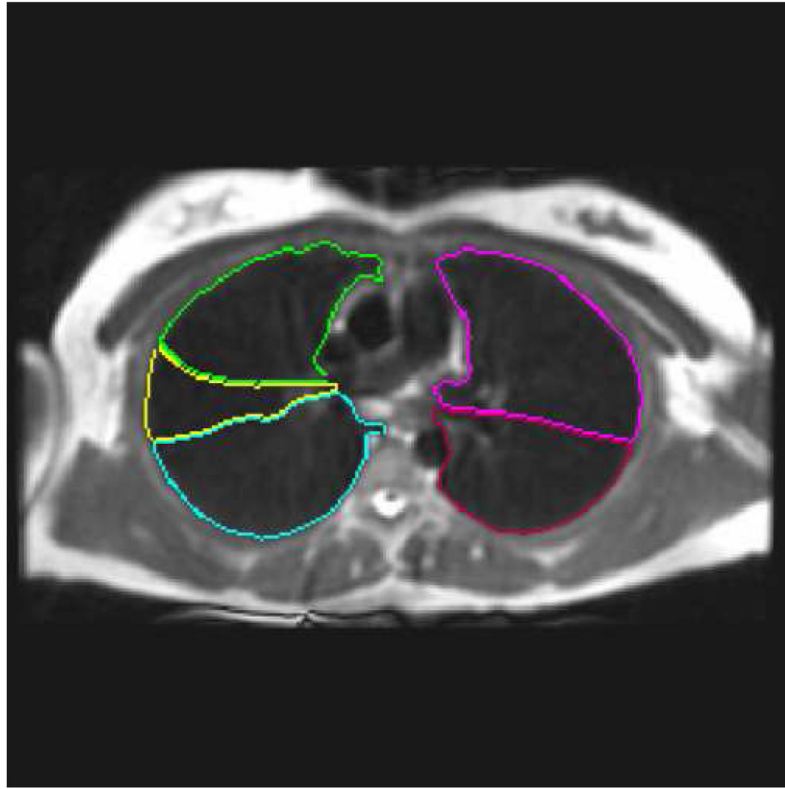
## References

1. Hartert TV, Peebles RS Jr. Epidemiology of asthma: the year in review. *Curr Opin Pulm Med* 2000;6(1):4-9. [PubMed: 10608418]
2. Sears MR, Greene JM, Willan AR, Wiecek EM, Taylor DR, Flannery EM, Cowan JO, Herbison GP, Silva PA, Poulton R. A Longitudinal, Population-Based, Cohort Study of Childhood Asthma Followed to Adulthood. *The New England Journal of Medicine* 2003;349:1414-1422. [PubMed: 14534334]
3. Postma DS, Timens W. Remodeling in asthma and chronic obstructive pulmonary disease. *Proc Am Thorac Soc* 2006;3(5):434-439. [PubMed: 16799088]
4. Permutt S. Current status of functional pulmonary imaging. *Acad Radiol* 2005;12(11):1359-1361. [PubMed: 16253847]
5. Haczku A, Emami K, Fischer MC, Kadlecsek S, Ishii M, Panettieri RA, Rizi RR. Hyperpolarized <sup>3</sup>He MRI in asthma measurements of regional ventilation following allergic sensitization and challenge in mice--preliminary results. *Acad Radiol* 2005;12(11):1362-1370. [PubMed: 16253848]
6. Holmes JH, Sorkness RL, Meibom SK, Sundaram SK, Perlman SB, Converse AK, Pyzalski RW, Hahn AD, Korosec FR, Grist TM, Fain SB. Noninvasive mapping of regional response to segmental allergen challenge using magnetic resonance imaging and [<sup>18</sup>F]fluorodeoxyglucose positron emission tomography. *Magn Reson Med* 2005;53(6):1243-1250. [PubMed: 15906295]
7. Holmes JH, Korosec FR, Du J, O'Halloran RL, Sorkness RL, Grist TM, Kuhlman JE, Fain SB. Imaging of lung ventilation and respiratory dynamics in a single ventilation cycle using hyperpolarized He-3 MRI. *J Magn Reson Imaging* 2007;26(3):630-636. [PubMed: 17685417]

8. Newman KB, Lynch DA, Newman LS, Ellegood D, Newell JD Jr. Quantitative computed tomography detects air trapping due to asthma. *Chest* 1994;106(1):105–109. [PubMed: 8020254]
9. Gono H, Fujimoto K, Kawakami S, Kubo K. Evaluation of airway wall thickness and air trapping by HRCT in asymptomatic asthma. *Eur Respir J* 2003;22(6):965–971. [PubMed: 14680087]
10. Ueda T, Niimi A, Matsumoto H, Takemura M, Hirai T, Yamaguchi M, Matsuoka H, Jinnai M, Muro S, Chin K, Mishima M. Role of small airways in asthma: investigation using high-resolution computed tomography. *J Allergy Clin Immunol* 2006;118(5):1019–1025. [PubMed: 17088124]
11. King GG, Eberl S, Salome CM, Young IH, Woolcock AJ. Differences in Airway Closure between Normal and Asthmatic Subjects Measured with Single-Photon Emission Computed Tomography and Technegas. *Am J Respir Crit Care Med* 1998;158:1900–1906. [PubMed: 9847284]
12. Harris RS, Winkler T, Tgavalekos N, Musch G, Melo MF, Schroeder T, Chang Y, Venegas JG. Regional pulmonary perfusion, inflation, and ventilation defects in bronchoconstricted patients with asthma. *Am J Respir Crit Care Med* 2006;174(3):245–253. [PubMed: 16690973]
13. Samee S, Altes T, Powers P, Lange Ed, Knight-Scott J, Rakes G, Mugler J, Ciambotti J, Alford B, Brookeman J, Platts-Mills T. Imaging the lungs in asthmatic patients by using hyperpolarized helium-3 magnetic resonance: Assessment of response to methacholine and exercise challenge. *Journal of Allergy and Clinical Immunology* 2003;111:1205–1211. [PubMed: 12789218]
14. de Lange EE, Altes TA, Patrie JT, Gaare JD, Knake JJ, Mugler JP 3rd, Platts-Mills TA. Evaluation of asthma with hyperpolarized helium-3 MRI: correlation with clinical severity and spirometry. *Chest* 2006;130(4):1055–1062. [PubMed: 17035438]
15. Hoffman EA, van Beek E. Hyperpolarized media MR imaging--expanding the boundaries? *Acad Radiol* 2006;13(8):929–931. [PubMed: 16843844]
16. de Lange EE, Altes TA, Patrie JT, Parmar J, Brookeman JR, Mugler JP 3rd, Platts-Mills TA. The variability of regional airflow obstruction within the lungs of patients with asthma: assessment with hyperpolarized helium-3 magnetic resonance imaging. *J Allergy Clin Immunol* 2007;119(5):1072–1078. [PubMed: 17353032]
17. Woodhouse N, Wild JM, Paley MN, Fischele S, Said Z, Swift AJ, van Beek EJ. Combined helium-3/proton magnetic resonance imaging measurement of ventilated lung volumes in smokers compared to never-smokers. *J Magn Reson Imaging* 2005;21(4):365–369. [PubMed: 15779032]
18. NIH-NHLBI. Expert Panel Report: Guidelines for the Diagnosis and Management of Asthma. EPR-Update 2002 of NIH Publication 97-4051 ed. Volume 2002: NIH/NHLBI; 2002.
19. Moore WC, Bleecker ER, Curran-Everett D, Erzurum SC, Ameredes BT, Bacharier L, Calhoun WJ, Castro M, Chung KF, Clark MP, Dweik RA, Fitzpatrick AM, Gaston B, Hew M, Hussain I, Jarjour NN, Israel E, Levy BD, Murphy JR, Peters SP, Teague WG, Meyers DA, Busse WW, Wenzel SE. Characterization of the severe asthma phenotype by the National Heart, Lung, and Blood Institute's Severe Asthma Research Program. *J Allergy Clin Immunol* 2007;119(2):405–413. [PubMed: 17291857]
20. Miller MR, Hankinson J, Brusasco V, Burgos F, Casaburi R, Coates A, Crapo R, Enright P, van der Grinten CP, Gustafsson P, Jensen R, Johnson DC, MacIntyre N, McKay R, Navajas D, Pedersen OF, Pellegrino R, Viegi G, Wanger J. Standardisation of spirometry. *Eur Respir J* 2005;26(2):319–338. [PubMed: 16055882]
21. Wanger J, Clausen JL, Coates A, Pedersen OF, Brusasco V, Burgos F, Casaburi R, Crapo R, Enright P, van der Grinten CP, Gustafsson P, Hankinson J, Jensen R, Johnson D, Macintyre N, McKay R, Miller MR, Navajas D, Pellegrino R, Viegi G. Standardisation of the measurement of lung volumes. *Eur Respir J* 2005;26(3):511–522. [PubMed: 16135736]
22. Hankinson JL, Odencrantz JR, Fedan KB. Spirometric reference values from a sample of the general U.S. population. *Am J Respir Crit Care Med* 1999;159(1):179–187. [PubMed: 9872837]
23. Stocks J, Quanjer PH. Reference values for residual volume, functional residual capacity and total lung capacity. *ATS Workshop on Lung Volume Measurements. Official Statement of The European Respiratory Society. Eur Respir J* 1995;8(3):492–506. [PubMed: 7789503]
24. Lung function testing: selection of reference values and interpretative strategies. *American Thoracic Society. Am Rev Respir Dis* 1991;144(5):1202–1218.



25. Miller GW, Altes TA, Brookeman JR, De Lange EE, Mugler JP 3rd. Hyperpolarized  $^3\text{He}$  lung ventilation imaging with B1-inhomogeneity correction in a single breath-hold scan. *Magma* 2004;16(5):218–226. [PubMed: 15108030]
26. Salerno M, Altes T, Brookeman J, Lange Ed, Mugler J. Dynamic spiral MRI of pulmonary gas flow using hyperpolarized  $^3\text{He}$ : preliminary studies in healthy and diseased lungs. *Magn Reson in Med* 2001;46:667–677. [PubMed: 11590642]
27. Wild J, Paley M, Kasuboski L, Swift A, Fichelle S, Woodhouse N, Griffiths P, Beek Ev. Dynamic radial projection MRI of inhaled hyperpolarized  $^3\text{He}$  gas. *Magn Reson Med* 2003;49(6):991–997. [PubMed: 12768575]
28. Holmes J, O'Halloran R, Brodsky E, Jung Y, Block W, Fain S. 3D Hyperpolarized He-3 MRI of Ventilation Using a Multi-Echo Projection Acquisition. *Magn Reson Med*. 2007Submitted



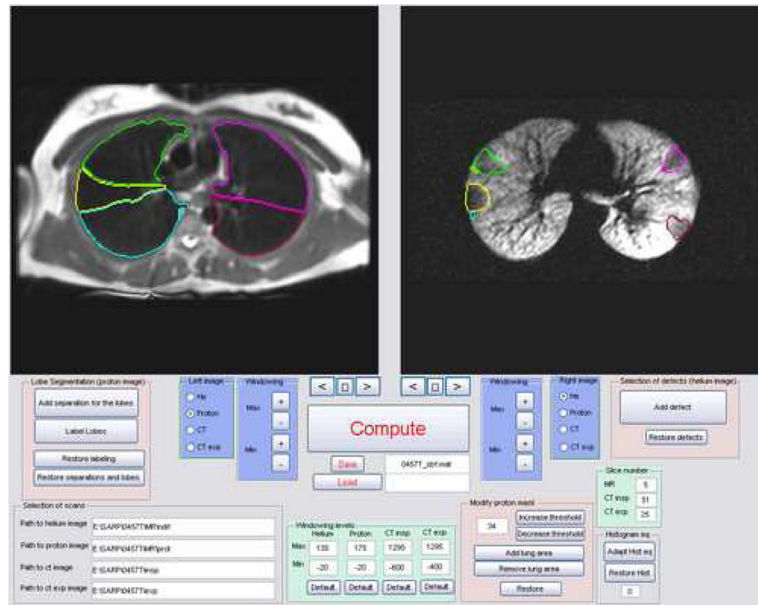


**Figure 1.**

(a) Segmented lung lobes (color code: yellow = right middle lobe, green = right upper lobe, blue = right lower lobe, magenta = left upper lobe, and red = left lower lobe) overlain on fast spin-echo (FSE) conventional proton MRI of the lung parenchyma acquired with the FSE sequence (Table 2). (b) Corresponding inspiratory MDCT slice (a) used for segmenting the lung lobes in (a). MDCT image in (b)  $512 \times 512$ , reconstructed at 0.5 cm thickness, using parameters summarized in Table 1. (c) Graphic user interface display with equivalent proton MRI and HP MRI slices with segmented lung lobes as described in (a). The HP MR image of ventilation in the right panel of (c) depicts ventilation defects segmented with lobe location marked using the same color code and was acquired with a GRE sequence and parameters summarized in Table 2.

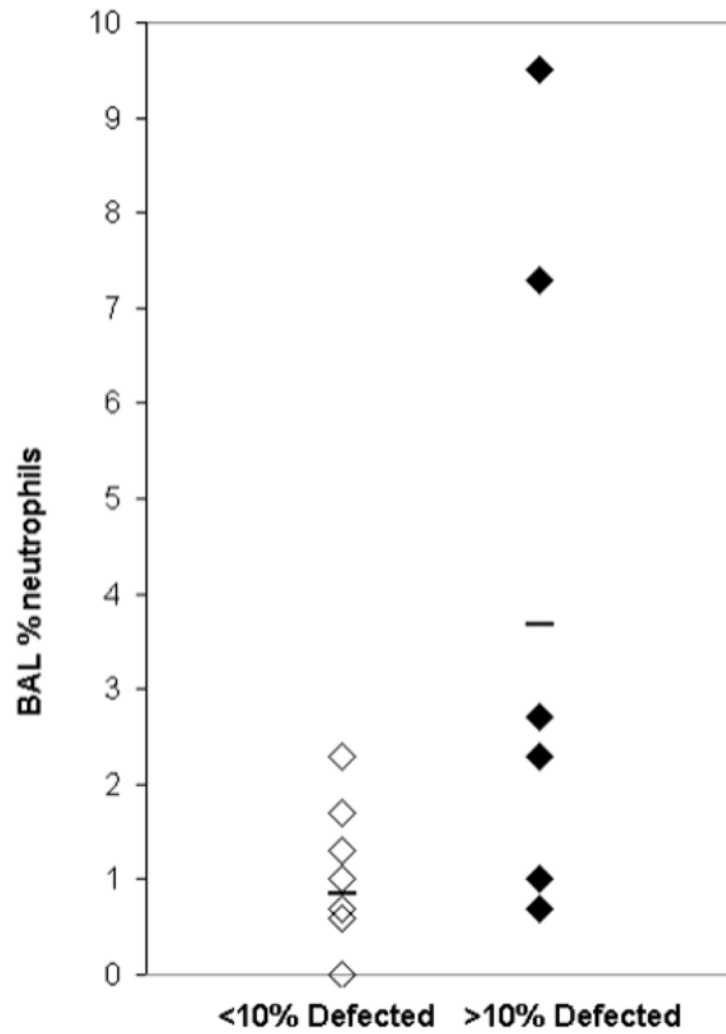


**Figure 2.** Scatter plot of high and low defected lobes showing increased % neutrophils ( $p = 0.03$ ) in lobes sampled with BAL and greater than 10% Defect Volume compared with lobes with less than 10% Defect Volume.

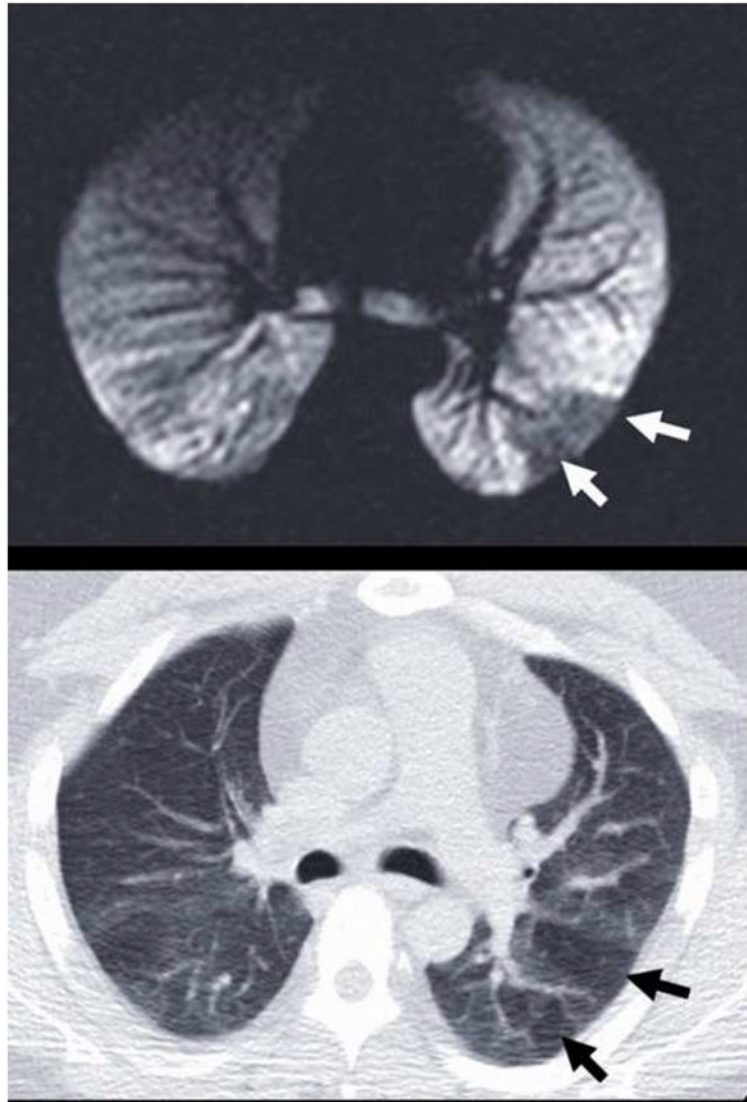


**Figure 3.** Typical example of the observed spatial correspondence (a) between ventilation defects on HP MRI (white arrows) and (b) hyperlucency on MDCT (black arrows). These defects in the left lower lobe reflect obstructive physiology at different lung volumes: 15% of TLC for HP MRI in (a) and FRC for expiratory MDCT in (b).

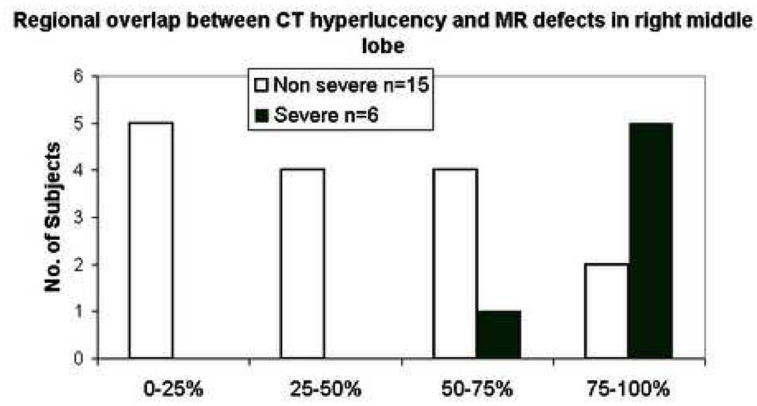


**Figure 4.** Qualitative distribution of regional overlap scores in the right middle lobe showing increased overlap between ventilation defects on HP MRI with hyperlucency on MDCT for subjects with severe vs. non-severe asthma.

**Table 1**

## MDCT Scan Parameters

Parameter	16 Detector	64 Detector
Collimation	1.25 mm	1.25 mm
Pitch	1.675	0.984
Source Current/Voltage	50 mA/120 kVp	50 mA/120 kVp
Gantry Speed	0.5 s/rotation	
Matrix	512 × 512	
Lung Volume	FRC (expiratory) and TLC (inspiratory)	
Reconstruction Kernel	"Standard" and "Lung"	
Reconstructed Slice Thickness	0.625 mm (quantitative) and 5 mm (qualitative)	

**Table 2**

## MRI Scan Parameters

Parameter	T1-Weighted Fast Spin Echo	Hyperpolarized $^3\text{He}$ MRI
TR/TE	$\infty/8$ ms	8.4/3.1 ms
Flip Angle	90°	7°
Bandwidth	31.25 kHz	31.25 kHz
Acquisition Matrix	128 × 64	128 × 128
Imaging Time	7–8 s	18–24 s
Axial plane FOV	32–38 × 24–29 cm <sup>2</sup>	
Slice FOV	13–19 × 1.5 cm slices	



**Table 3**

Statistical summary (Mean  $\pm$  Standard Deviation) of image metrics and pulmonary function with asthma severity for subjects included in the regional analysis.

Parameter	Severe (N=6)	Non-severe (N=15)	Overall (N=21)
Defect Score	16.7 $\pm$ 12.3	11.0 $\pm$ 9.5	12.6 $\pm$ 10.4
Percent Defect Volume (%)	7.6 $\pm$ 4.2	5.4 $\pm$ 4.5	6.0 $\pm$ 4.4
Expiratory densitometry:			
Percent below -850 HU	4.7 $\pm$ 2.1	8.0 $\pm$ 7.3	7.0 $\pm$ 6.4
Percent below -910 HU	0.9 $\pm$ 1.0	1.5 $\pm$ 1.7	1.3 $\pm$ 1.6
Percent below -950 HU	0.3 $\pm$ 0.5	0.4 $\pm$ 0.7	0.4 $\pm$ 0.6
FEV1 (% predicted)	82.7 $\pm$ 11.1	91.5 $\pm$ 15.1	89.0 $\pm$ 14.3
FEF25-75 (% predicted)	71.7 $\pm$ 36.3	69.4 $\pm$ 23.4	70.0 $\pm$ 26.8
FEV1/FVC (% predicted)	94.4 $\pm$ 13.6	89.2 $\pm$ 8.6	90.7 $\pm$ 10.2
RV/TLC	0.323 $\pm$ 0.098	0.308 $\pm$ 0.052	0.312 $\pm$ 0.066
BAL:			
% Neutrophils	0.86 $\pm$ 0.86	2.48 $\pm$ 2.93	2.01 $\pm$ 2.58
% Eosinophils	0.74 $\pm$ 0.73	0.63 $\pm$ 0.67	0.66 $\pm$ 0.67
% Macrophage	91.3 $\pm$ 2.9	85.5 $\pm$ 11.2	87.2 $\pm$ 9.8

**Table 4**  
Spearman correlations between image, pulmonary lung function, and BAL measures.

Parameter	Correlate				
	FEV1 % predicted	FEV1/FVC % predicted	FEF25-75 % predicted	RV/TLC % predicted	BAL % Neutrophils
Defect Score: (n = 21)	-0.76 p=0.0002	-0.24 p = 0.31	-0.54 p=0.03	0.58 p = 0.02	0.23 p = 0.17
BAL Total Neutrophils (10 <sup>6</sup> cells)					0.06 p = 0.82
Expiratory Densitometry: (n = 45)					
Percent below -850 HU	-0.37 p = 0.04	-0.52 p = 0.02	-0.55 p = 0.002	0.53 p = 0.003	0.16 p = 0.54
% Defect Volume:					
Whole Lung (n = 21)	-0.57 p = 0.007	-0.23 p = 0.31	-0.43 p = 0.08	0.37 p = 0.15	0.41 p = 0.11
@BAL Site (n = 17)	-	-	-	-	0.68 p = 0.0039
					0.61 p = 0.0125